Journal of Materials Chemistry C

Accepted Manuscript

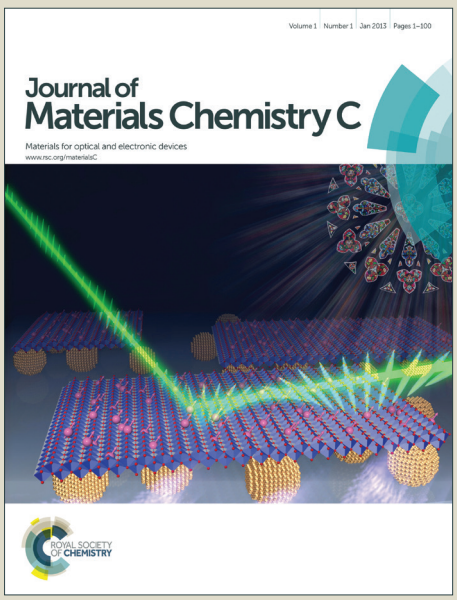

ROYAL SOCIETY OF CHEMISTRY

www.rsc.org/materialsC

Synthesis of upconversion $NaYF_4:Yb^{3+},Er^{3+}$ particles with enhanced luminescent intensity through control of morphology and phase

Min Lin[a,b], Ying Zhao[b], Ming Liu[c], MuShu Qiu[a,b], YuQing Dong[b], ZhenFeng Duan[d], Tian Jian Lu[b#], Feng Xu[a,b#]

[a] *The Key Laboratory of Biomedical Information Engineering, Ministry of Education, School of Life Science and Technology, Xi'an Jiaotong University, Xi'an 710049, P.R. China*

[b] *Bioinspired Engineering and Biomechanics Center (BEBC), Xi'an Jiaotong University, Xi'an, P.R. China 710049*

[c] *Electronic Materials Research Laboratory, Key Laboratory of the Ministry of Education & International Center for Dielectric Research, Xi'an Jiaotong University, Xi'an 710049, China*

[d] *Center for Sarcoma and Connective Tissue Oncology, Massachusetts General Hospital, Harvard Medical School, MA, USA*

[#] *Corresponding author: tjlu@mail.xjtu.edu.cn, fengxu@mail.xjtu.edu.cn*

Abstract: Preparation of well-defined $NaYF_4$ crystals with bright upconversion emission remains a major challenge. The complicated chemical reactions, as well as the effect of structures, phase and morphology on emission efficiency requires finely tuning of multiple parameters during the growth of $NaYF_4$ crystal. In this study, we successfully synthesized $NaYF_4:Yb^{3+},Er^{3+}$ microcrystals with well-controlled morphologies (*e.g.*, sphere, tube) and enhanced luminescent intensity through tuning pH values and ions concentrations in the initial reaction solution. With increasing reaction time, the phase of $NaYF_4:Yb^{3+},Er^{3+}$ changes from cubic to hexagonal, while the morphology follows the change from spheres to microtubes and then to microrods. Upon excitation by 980 nm infrared light, hexagonal $NaYF_4:Yb^{3+},Er^{3+}$ microtubes show a significant enhancement in green upconversion emission, which is

much stronger than that observed in other particles with various morphologies. This phase and morphology dependent strong upconversion emission holds great potential for applications in photonic devices and bioanalyses.

1. Introduction

As one of the most important fluorescent materials, lanthanide-doped upconversion materials have attracted increasing interest due to their capability of absorbing and converting lower energy excitations with near-infrared long wavelength to higher energy emissions with short wavelength [1-6]. This unique feature renders these materials with many advantages over organic dyes and quantum dots in biological applications, such as enhanced tissue penetration [7, 8], weak autofluorescence [9], improved resistance to photobleaching [10], and lower cytotoxicity [11]. Thus, the lanthanide-doped upconversion materials find widespread applications in biomedicine, such as biological imaging [3, 12], biological sensing/detection [10, 13], development of point-of-care devices and drug delivery [14-16]. For these applications, the enhanced detection signals are highly demanded [17, 18]. Therefore, synthesis of lanthanide-doped upconversion materials with superior luminescent property has become the focus of interest recently.

Rare earth oxides and fluorides have been widely used as host crystals for the synthesis of lanthanide-doped upconversion materials [19]. Among them, β-$NaYF_4$ is one of the most efficient host lattices for generating upconversion emission, thus attracting intensive study in the field of materials science [20]. Rational control over morphology and phase allows manipulation of micro and nanocrystals with desired properties. The understanding of how the luminescent property changes with morphology and phase is of great significance in the design of upconversion materials. Therefore, numerous investigations have been devoted to the synthesis of lanthanide-doped β- and α- $NaYF_4$ micro and nanocrystals. Hydrothermal route has been successfully employed to synthesize lanthanide-doped β-$NaYF_4$ with various morphologies, such as nanosphere [21], nanowires [22], pindle-like microcrystal [23], microrod [24], microprim [25], and octadecahedron [26]. The particle morphologies have been found to have significant effect on the fluorescence property of lanthanide-doped upconversion materials [20, 24, 27]. For example, β-$NaLuF_4$:Yb^{3+},Er^{3+} [28] and

β-$NaYbF_4$:Tm^{3+} with microtube shape [29] possess higher fluorescent intensity than those with other morphologies (*e.g.*, cube, rod and prim). Therefore, it is desirable to synthesize lanthanide-doped $NaYF_4$ with microtube shape to achieve enhanced fluorescent intensity. Although the synthesis of β-$NaYF_4$:Yb^{3+},Er^{3+} microtubes has been achieved by using ethylenediamine tetraacetic acid as an organic surfactant via hydrothermal method [30] and via molten salt method [31], these two methods either involve organic substance or require the high reaction temperature (*e.g.*, 350 ℃). In addition, the mechanism underlying the morphology evolution and the morphology dependent emission intensity is still not clear. Therefore, there is still an unmet need for developing an environment-friendly method with mild reaction condition to synthesize lanthanide-doped upconversion $NaYF_4$ microtube.

In this study, we have developed a facile and effective hydrothermal method to synthesize $NaYF_4$:Yb^{3+},Er^{3+} microtubes with enhanced luminescent intensity in ultrapure water. Precise control over the particle phase and morphology has been achieved by simply tuning pH value in the initial solution. The morphology evolution and the growth mechanism of preparing $NaYF_4$:Yb^{3+},Er^{3+} have been studied by controlling the reaction time. The upconversion photoluminescent properties of β-$NaYF_4$:Yb^{3+},Er^{3+} with different morphologies and the possible mechanism that β-$NaYF_4$:Yb^{3+},Er^{3+} microtubes possess the highest luminescent intensity are presented as well.

2. Experimental section

2.1 Preparation

$Y(NO_3)_3 \cdot 6H_2O$, $Yb(NO_3)_3 \cdot 5H_2O$ and $Er(NO_3)_3 \cdot 5H_2O$ were purchased from Alfa Aesar (UK). NaF (with purity of 99.99%) and HNO_3 were purchased from Tianjin Yong Sheng Fine Chemical Co., Ltd. All of these reagents were used as received without any further purification. We first prepared solutions with three different concentrations of 0.00131, 0.00022 and 0.00011 mol mL^{-1} by dissolving 25g

$Y(NO_3)_3 \cdot 6H_2O$, 10g $Yb(NO_3)_3 \cdot 5H_2O$, 25g $Er(NO_3)_3 \cdot 5H_2O$ into a volumetric flask. The mixture of NaF and Ln $(NO_3)_3$ (Ln^{3+}=Y^{3+}, Yb^{3+}, Er^{3+}) with a molar ratio of 16.0 :1. was put into a 50 mL Teflon lined autoclave. The molar ratio of Y:Yb:Er equals 80:18:2. After 30 min magnetic stirring, 30 mL ultrapure water was added. The pH value was adjusted by dripping a solution of concentrated nitric acid: ultrapure water = 2.0: 1.0 under continuous stirring. The reaction mixture was sealed in Teflon lined autoclave which was kept in a stainless steel autoclave, and maintained in oven at 180 ℃ for 2h, 8h and 14h, respectively. Then the autoclave was cooled to room temperature naturally, and the product was separated by centrifugation, washed with ultrapure water and ethanol in sequence for three times, and then dried in air at 60 ℃ for 12 h.

2.2 Characterization

The as-prepared samples were characterized by Power X-ray diffraction (XRD) on a XRD-7000 diffractometer with graphite-monochromatized Cu Kα radiation. The morphologies of the samples were obtained by using a field emission scanning electron microscope (SEM) on a JSM-6700F. The transmission electron microscopy (TEM) and the high-resolution transmission electron microscopy (HRTEM) images were taken by JEM 2100 instrument at the accelerating voltage of 200 kV. The upconversion emission spectra were recorded by using a spectrophotometer (QuantaMasterTM40) under external excitation of a 250 mW 980 nm laser diode (RGB Lasersystems). All the measurements were performed at room temperature.

3. Results and discussion

3.1 pH dependent phase and morphology

A. YF_3 octahedron. To obtain the crystallography of the synthesized particles, we performed powder XRD for products prepared at 180 ℃ for 14 h under various pH conditions of pH =1.5, 2.0, 2.5 (Fig. 1). When the pH value is close to 1.5, the diffraction peaks of the sample can be identified as YF_3 (JCPDS No. 32-1431) showing an orthorhombic phase (Fig. 1a). Whereas, the reflection peaks of samples

from pH of near 2.0 and 2.5 are identified as pure hexagonal-phased $NaYF_4$ (β-$NaYF_4$) (Fig. 1b-c), which agree well with the literature values (JCPDS No. 16-0334), except the sample from pH=2.0 that has some weak peaks corresponding to cubic-phased $NaYF_4$ (α-$NaYF_4$) (JCPDS No. 06-0342). It is noteworthy that the XRD patterns also indicate that there are differences in the relative intensities of the (100), (110), (101), and (201) peaks for the samples from pH=2.0 and 2.5, indicating that there may exit different preferential orientation growth.

The morphology of the synthesized particles was characterized with SEM (Fig. 2a). We observed octahedral microparticles with average edge length of ~25 μm for samples from pH=1.5. Higher magnification image of the octahedral microparticles shows sharp edge and fairly smooth surface (Fig. 2b). The selected area electron diffraction (SAED) pattern of the spot indicates a single crystalline nature of the octahedral microparticles (Fig. 2c). The HRTEM image (Fig. 2d) shows an interplanar distance of 0.198 nm, which can be ascribed to the lattice spacing of (112) planes of YF_3.

B. β-$NaYF_4$:Yb^{3+},Er^{3+} microtubes. At pH=2.0, the integral morphology of $NaYF_4$:Yb^{3+},Er^{3+} shows tube shape with outer diameters of 600 nm to 1.2 μm. The wall thickness varies from 170 to 380 nm and the length of the tubes range from 3.8 to 5.8 μm (Fig. 3a). The outer surface of the tubes forms a hexagonal prism and has broken ends. The TEM image also confirms the characteristics of $NaYF_4$:Yb^{3+},Er^{3+} microtubes (Fig. 3b). However, the inner structure can not be observed clearly in the TEM image due to the large thickness of the tube wall. The corresponding SAED pattern, which further convinced that the microtubes are single crystalline (Fig. 3c). The obvious lattice fringes in the HRTEM image (Fig. 3d) confirm the high crystallinity of the sample, which agrees well with the XRD results. The determined interplanar distance of 0.297 nm between the adjacent lattice planes (marked by the arrows) is in good agreement with the d_{110} spacing of hexagonal $NaYF_4$:Yb^{3+},Er^{3+}.

C. β-$NaYF_4$:Yb^{3+},Er^{3+} limb-like structure. Once the pH value increased to 2.5, the morphology of the product changed into pseudo-microtube structures with the average length of 2.6 μm and the diameter of 0.85 μm (Fig. 4a). Moreover, there is a small quantity of pseudo-microtube interconnecting from the centers to form a limb-like structure. Fig. 4b shows the TEM image of $NaYF_4$:Yb^{3+},Er^{3+}, but the entire sample is too large to show its inner structure clearly. The SAED pattern shown in Fig. 4c displays orderly arranged diffraction spots, indicating their single crystalline nature. The interplanar distance of 0.207 nm, which could be indexed to the d_{201} spacing of hexagonal $NaYF_4$:Yb^{3+},Er^{3+} (Fig. 4d).

3.2 The growth mechanism of Microtubes

To understand the formation and morphological evolution processes of the $NaYF_4$:Yb^{3+},Er^{3+} microtubes, we investigated the time-controlled evolution of $NaYF_4$:Yb^{3+},Er^{3+} microstructures. XRD pattern and SEM images of the samples prepared with reaction times of 0.5, 8and 14h are shown in Fig. 5. As the samples experience a $\alpha \rightarrow \beta$ transformation process, the morphologies evolve during the crystal growth accordingly. Through a set of experiments, the mechanism for the time-dependent morphology evolution is proposed, as shown in Fig. 6. In a very short reaction time (0.5h), the sample obtained is pure α-$NaYF_4$:Yb^{3+},Er^{3+} (Fig. 5a), which corresponds to spherical-like nanoparticles with a mean diameter of 115 nm (Fig. 5b). The α-$NaYF_4$:Yb^{3+},Er^{3+} seeds have isotropic unit cell structures, inducing an isotropic growth of particles. However, these α-$NaYF_4$:Yb^{3+},Er^{3+} are unstable and phase transformation takes place through a dissolution–nucleation process to form more stable β-$NaYF_4$:Yb^{3+},Er^{3+} (Fig. 5a). The similar formation mechanism has been reported for β-$NaYF_4$:Yb^{3+},Er^{3+} [32] and β-$NaLuF_4$:Yb^{3+},Er^{3+} [28]. When the reaction time is increased to 8 h, β-$NaYF_4$:Yb^{3+},Er^{3+} microtubes as well as a small amount of α-$NaYF_4$:Yb^{3+},Er^{3+} nanoparticles can be obtained (Fig. 5c). Different from the cubic phase, the β-$NaYF_4$:Yb^{3+},Er^{3+} possess an anisotropic unit cell structure, which leads to an anisotropic growth via a dissolution-reconstruction process to form a hexagonal cylinder. Subsequent fast growth on the edges leads to the under saturation of

substances in the centers and eventually produces β-$NaYF_4$:Yb^{3+},Er^{3+} microtubes with well-defined cross sections [28, 33-35]. Pure β-$NaYF_4$:Yb^{3+},Er^{3+} with a microtube morphology can be achieved when the reaction time is increased to 14 h. The morphology of these microtubes do not change much compared to those prepared at 8 h.

3.3 Upconversion luminescent properties

Upconversion luminescence spectrum of the as-prepared products at different pH values (pH = 1.5, 2.0 and 2.5) was acquired under the excitation of a 980 nm laser diode at room temperature. The experimental conditions (*e.g.*, excitation source, excitation intensity and concentration) remain the same for all the samples. Upconversion luminescence emission spectra of the YF_3:Yb^{3+},Er^{3+} with octahedral morphology and β-$NaYF_4$:Yb^{3+},Er^{3+} with microtubes and limb-like morphology are shown in Fig. 7. Upconversion emission peaks of green and red centered at 515/535 and 653 nm were observed, which can be assigned to the $^2H_{11/2}$/$^4S_{3/2}$→$^4I_{15/2}$ and $^4F_{9/2}$→$^4I_{15/2}$ transitions of Er^{3+} ions, respectively [30].

Based on the energy matching conditions, possible upconversion mechanisms for the Yb^{3+}/Er^{3+} co-doped $NaYF_4$ are discussed on the basis of the simplified energy level diagram as shown in Fig. 8. In the Yb^{3+}/Er^{3+} co-doped system, the pumping light with wavelength of 980 nm matches the $^2F_{7/2}$→$^2F_{5/2}$ transition within Yb^{3+} ion. After excitation, the $^2F_{5/2}$ (Yb^{3+}) transfers energy to Er^{3+} ion by populating the $^4I_{11/2}$ (Er^{3+}) level. A further excitation from $^4I_{11/2}$ (Er^{3+}) to $^4F_{7/2}$ (Er^{3+}) occurs after energy transfer from Yb^{3+} ion from a second photon absorption. Transition from $^4F_{7/2}$ (Er^{3+}) to $^2H_{11/2}$ (Er^{3+}) and $^4S_{3/2}$ (Er^{3+}) occurs by non-radiative energy decay process. Green emission at around 515 and 535 nm results separately from the transitions from $^2H_{11/2}$ (Er^{3+}) and $^4S_{3/2}$ (Er^{3+}) to the ground state $^4I_{15/2}$ (Er^{3+}). Red emission around 653 nm could be attributed to the transition between $^4F_{9/2}$ (Er^{3+}) and $^4I_{15/2}$ (Er^{3+}). The left inset in Fig. 7 shows a photography image for samples prepared under different pH values. From the

images, the green upconversion luminescence can be visually observed by the naked eyes. The right inset of Fig. 7 presents the variation of emission intensities as a function of the pH value in the samples. It is clear from the inset that the intensities change obviously with the pH value.

It should be noted that, in all the three samples, the upconversion spectra are similar in shape, and the emission bands differ only in the intensity. The microtubes exhibit the strongest emission intensity, while the octahedral show very weak emission intensity, and the relative intensity of the former is about 3 orders of magnitude higher than that of the latter. The difference between upconversion luminescent intensities could be attributed to the combined roles of phase, morphologies and particle size [24]. Based on the XRD patterns of the as-prepared products at different pH values (Fig. 1), β-$NaYF_4$ is more efficient host lattice than YF_3, so samples prepared under pH=2.0 and 2.5 have higher intensity then pH=1.5. Although the samples prepared under pH=2.0 (microtube) and 2.5 (limb-like structure) have the same β-$NaYF_4$ phase, the relative intensity of microtubes is almost 6 times as high as that of the limb-like structure. This phenomenon may be caused by the different particle size and morphologies. The microtubes sample has larger size as we discussed previously. With increasing crystal size, the Er^{3+} ion concentration on crystal surface reduces significantly resulting in lower surface defects and stronger emission [24].Moreover, microtubes have larger surface area (inner and outer surfaces) than limb-like structures. Larger surface area promotes the absorption efficiency under similar excitation condition, therefore generating higher luminescent intensity.

Since it has been demonstrated that ions concentrations have significant influence on the morphology of the as prepared products [27, 36]. This will thus affect the luminescent intensity. The influence of F^-/Ln^{3+} (Ln^{3+}=Y^{3+}, Yb^{3+}, Er^{3+}) ratio on the morphology, phase and the luminescent intensity of the obtained products were therefore discussed and were summarized in the support information (see supporting information).

4. Conclusion

In this paper, we have developed a facile hydrothermal route for synthesis of Yttrium fluoride compounds with different morphologies and crystal phases. Without any organic additives, the β-$NaYF_4$:Yb^{3+},Er^{3+} microtubes, β-$NaYF_4$:Yb^{3+},Er^{3+} limb-like structures and YF_3 octahedra can be obtained by simply tuning the pH values in the initial solution. The possible mechanism for the formation of β-$NaYF_4$:Yb^{3+},Er^{3+} microtubes has been studied by performing time-dependent morphology evolution experiments. Moreover, investigation of upconversion spectra of the products under the same measurement condition reveals that β-$NaYF_4$:Yb^{3+},Er^{3+}microtubes show considerably stronger luminescent intensity of around 6 times and 3 orders of magnitude than β-$NaYF_4$:Yb^{3+},Er^{3+} limb-like structure and YF_3:Yb^{3+},Er^{3+} octahedra, respectively. The enhanced luminescent intensity was attributed to the enlarged crystal size and absorption efficiency of β-$NaYF_4$:Yb^{3+},Er^{3+} microtubes. The facile and environmentally friendly method for the synthesis of one-dimensional microtubes will benefit controlled synthesis of other lanthanide-doped rare earth fluoride microtubes with enhanced luminescent intensity for potential application as bioanalyses and optical devices.

Acknowledgment

This work was financially supported by the National Natural Science Foundation of China (11372243), the National 111 Project of China (B06024), the Major International Joint Research Program of China (11120101002), the Key (Key grant) Project of Chinese Ministry of Education (313045), the South Wisdom Valley Innovative Research Team Program, International Science & Technology Cooperation Program of China (2013DFG02930), National Instrumentation Program (2013YQ190467), and the Fundamental Research Funds for the Central Universities (2012jdhz46). FX was also partially supported by the China Young 1000-Talent

Program and Program for New Century Excellent Talents in University (NCET-12-0437).

References

1. J. Shen, L. Zhao and G. Han, *Adv Drug Deliv Rev*, 2013, **65**, 744-755.
2. Z. Gu, L. Yan, G. Tian, S. Li, Z. Chai and Y. Zhao, *Advanced Materials*, 2013, **25**, 3758-3779.
3. J. Zhou, Z. Liu and F. Li, *Chem Soc Rev*, 2012, **41**, 1323-1349.
4. D. K. Chatterjee, M. K. Gnanasammandhan and Y. Zhang, *Small*, 2010, **6**, 2781-2795.
5. H. Dong, L.-D. Sun and C.-H. Yan, *Nanoscale*, 2013, **5**, 5703-5714.
6. M. Lin, Y. Zhao, S. Wang, M. Liu, Z. Duan, Y. Chen, F. Li, F. Xu and T. Lu, *Biotechnol Adv*, 2012, **30**, 1551-1561.
7. D. K. Chatterjee and Z. Yong, *Nanomedicine*, 2008, **3**, 73-82.
8. D. K. Chatterjee, A. J. Rufaihah and Y. Zhang, *Biomaterials*, 2008, **29**, 937-943.
9. N. M. Idris, Z. Q. Li, L. Ye, E. K. W. Sim, R. Mahendran, P. C. L. Ho and Y. Zhang, *Biomaterials*, 2009, **30**, 5104-5113.
10. F. Zhang, Q. Shi, Y. Zhang, Y. Shi, K. Ding, D. Zhao and G. D. Stucky, *Advanced Materials*, 2011, **23**, 3775-3779.
11. A. R. Jalil and Y. Zhang, *Biomaterials*, 2008, **29**, 4122-4128.
12. Q. Dou, N. M. Idris and Y. Zhang, *Biomaterials*, 2013, **34**, 1722-1731.
13. Y. Liu, D. Tu, H. Zhu, E. Ma and X. Chen, *Nanoscale*, 2013, **5**, 1369-1384.
14. C. Wang, L. Cheng and Z. Liu, *Biomaterials*, 2011, **32**, 1110-1120.
15. D. Yang, X. Kang, P. Ma, Y. Dai, Z. Hou, Z. Cheng, C. Li and J. Lin, *Biomaterials*, 2013, **34**, 1601-1612.
16. P. L. A. M. Corstjens, L. van Lieshout, M. Zuiderwijk, D. Kornelis, H. J. Tanke, A. M. Deelder and G. J. van Dam, *J. Clin. Microbiol.*, 2008, **46**, 171-176.
17. Ramesh Kattumenu, Chang H. Lee, Limei Tian, Michael E. McConney and S. Singamaneni, *J. Mater. Chem.*, 2011, **21**, 15218-15223.
18. H. Cui, C. Hong, A. Ying, X. Yang and S. Ren, *ACS Nano*, 2013, **7**, 7805-7811.
19. F. Wang and X. G. Liu, *Chemical Society Reviews*, 2009, **38**, 976-989.
20. Q. Dou and Y. Zhang, *Langmuir*, 2011, **27**, 13236-13241.
21. Y. Wang, R. Cai and Z. Liu, *Cryst Eng Comm*, 2011, **13**, 1772-1774.
22. D.-K. Ma, S.-M. Huang, Y.-Y. Yu, Y.-F. Xu and Y.-Q. Dong, *The Journal of Physical Chemistry C*, 2009, **113**, 8136-8142.
23. J. Zhuang, X. Yang, J. Fu, C. Liang, M. Wu, J. Wang and Q. Su, *Crystal Growth & Design*, 2013, **13**, 2292-2297.
24. S. Hao, G. Chen, H. Qiu, C. Xu, R. Fan, X. Meng and C. Yang, *Materials Chemistry and Physics*, 2012, **137**, 97-102.
25. Feng Tao, Feng Pan, Zhijun Wang, Weili Cai and L. Yao, *Cryst Eng Comm*, 2010, **12**, 4263-4267.
26. L. Gao, X. Ge, Z. Chai, G. Xu, X. Wang and C. Wang, *Nano Research*, 2009, **2**, 565-574.

27. X. Qu, H. K. Yang, G. Pan, J. W. Chung, B. K. Moon, B. C. Choi and J. H. Jeong, *Inorganic Chemistry*, 2011, **50**, 3387-3393.
28. C. Li, Z. Quan, P. Yang, S. Huang, H. Lian and J. Lin, *The Journal of Physical Chemistry C*, 2008, **112**, 13395-13404.
29. S. Zeng, G. Ren, W. Li, C. Xu and Q. Yang, *The Journal of Physical Chemistry C*, 2010, **114**, 10750-10754.
30. Zhuang, Liang, H. H. Y. Sung, Yang, Wu, I. D. Williams, Feng and Q. Su, *Inorganic Chemistry*, 2007, **46**, 5404-5410.
31. Xiao Zhang, Piaoping Yang, Chunxia Li, Dong Wang, Jie Xu, Shili Gai and Jun Lin, *Chem. Commun.*, 2011, **47**, 12143-12145.
32. Y. Chen, W. He, H. Wang, X. Hao, Y. Jiao, J. Lu and S.-e. Yang, *Journal of Luminescence*, 2012, **132**, 2404-2408.
33. X. Zhang, P. Yang, C. Li, D. Wang, J. Xu, S. Gai and J. Lin, *Chemical Communications*, 2011, **47**, 12143-12145.
34. N. N. P. Y. F. H. X. Z. S. G. C. L. J. Lin, *J. Mater. Chem*, 2012, **22**, 10889-10899.
35. C. Li, Z. Quan, P. Yang, J. Yang, H. Lian and J. Lin, *Journal of Materials Chemistry*, 2008, **18**, 1353-1361.
36. X. Qu, G. Pan, H. K. Yang, Y. Chen, J. W. Chung, B. K. Moon, B. C. Choi and J. H. Jeong, *Optical Materials*, 2012, **34**, 1007-1012.

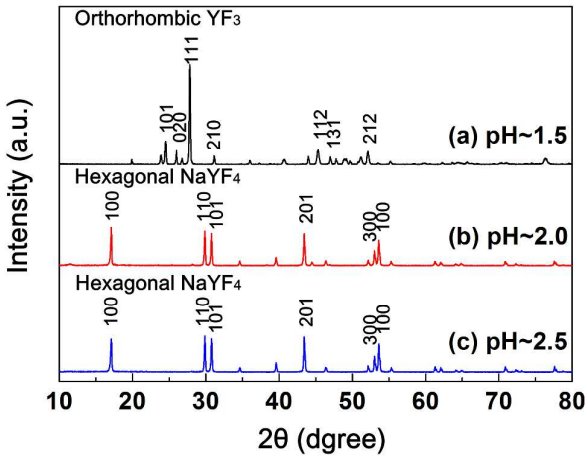

Fig. 1 XRD patterns of the as-prepared products at different pH values: (a) pH = 1.5; (b) pH=2.0; (c) pH=2.5.

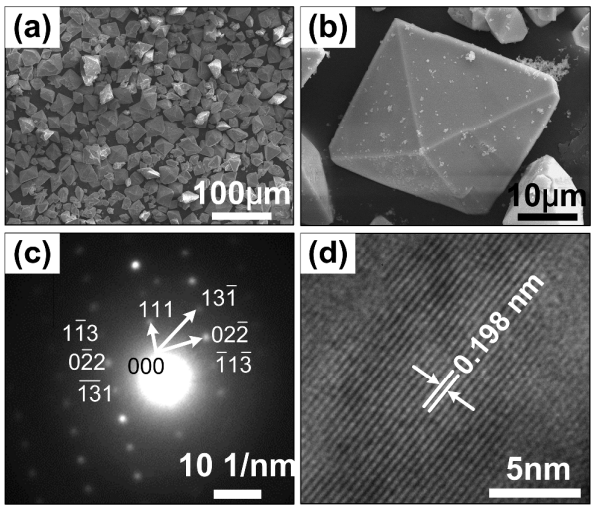

Fig. 2 Low and high-magnification SEM images (a) and (b), SAED image (c), HRTEM image (d) of YF_3 obtained at pH=1.5.

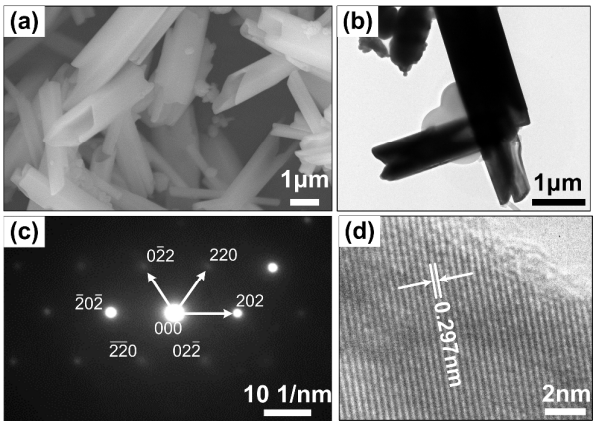

Fig. 3 SEM images (a), TEM images (b),SAED image (c), HRTEM image (d) of $NaYF_4$:Yb^{3+},Er^{3+}obtained at pH=2.0.

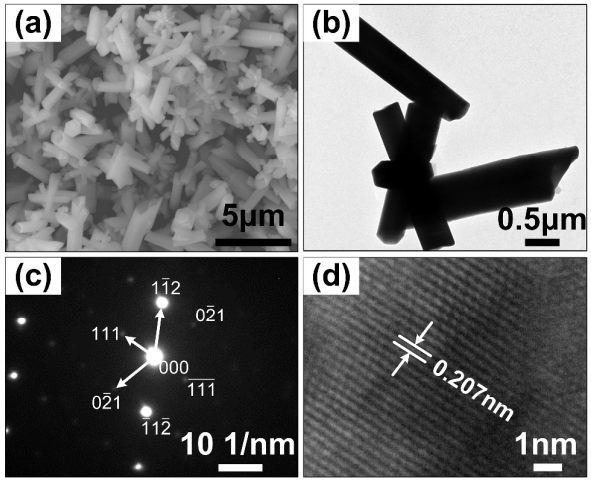

Fig. 4 SEM image (a), TEM image (b), SAED image (c), HRTEM image (d) of $NaYF_4:Yb^{3+},Er^{3+}$obtained at pH=2.5.

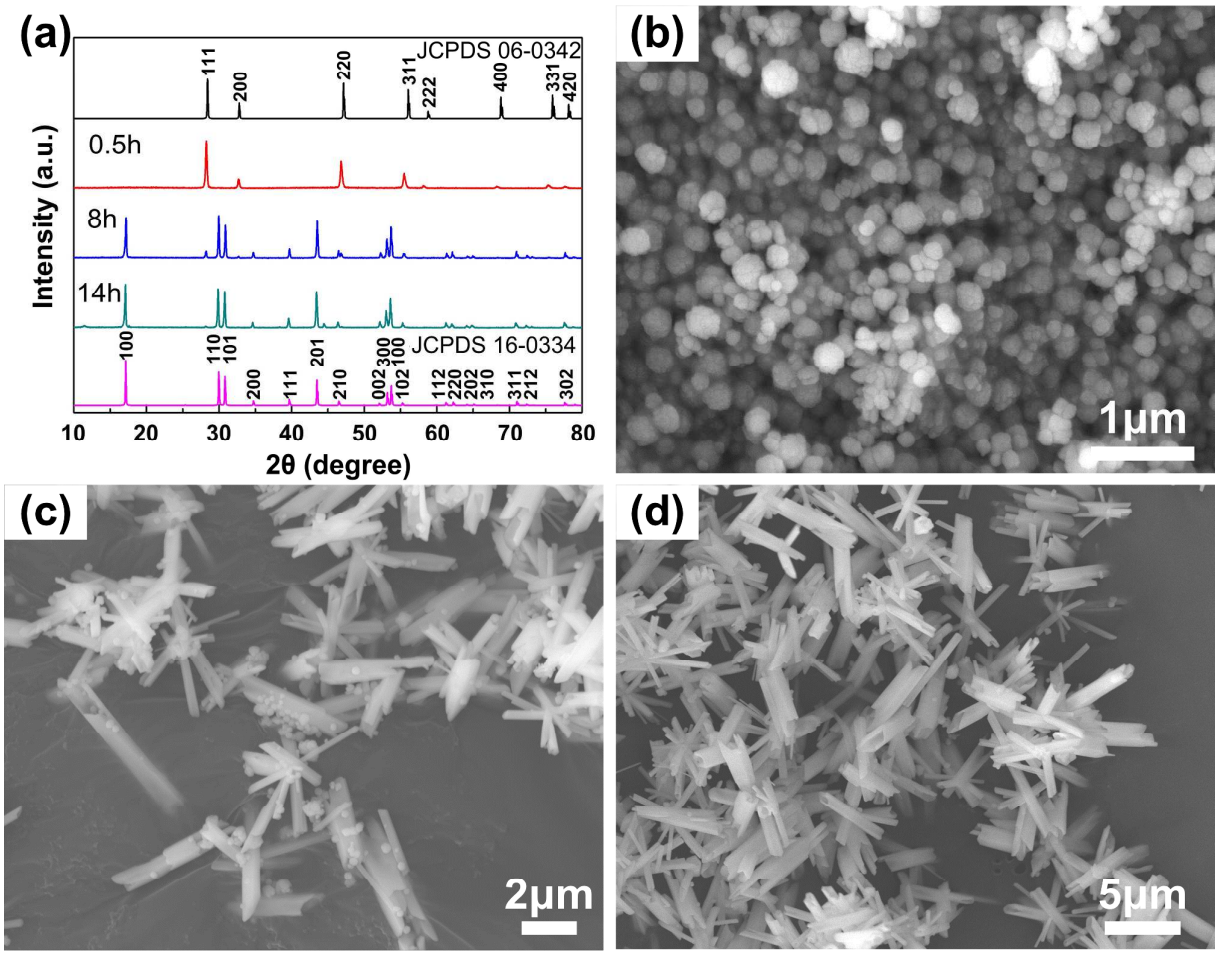

Fig. 5 XRD patterns (a) and SEM images of the $NaYF_4:Yb^{3+},Er^{3+}$ synthesized with differing reaction times of 0.5, 8 and 14h.

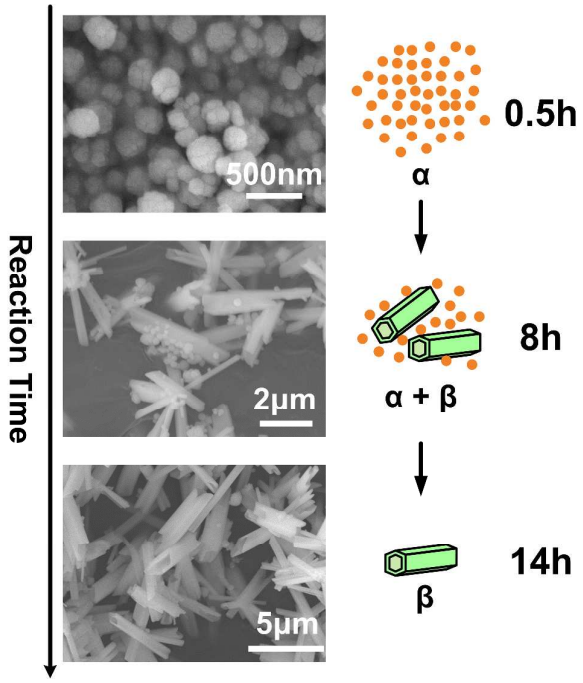

Fig. 6 Schematic diagram of the proposed formation and evolution process of the $NaYF_4:Yb^{3+},Er^{3+}$microtubes crystals.

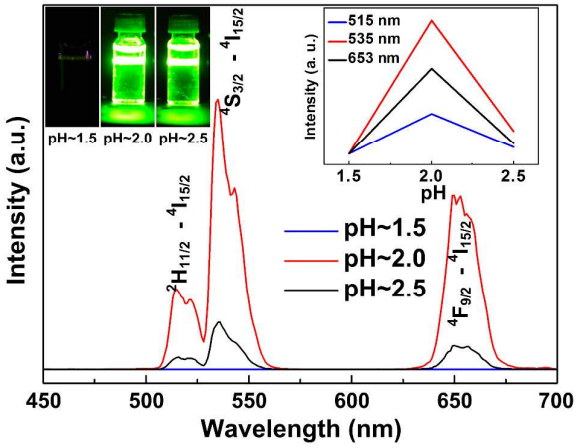

Fig. 7 Upconversion luminescence spectrum of the products prepared at different pH values under excitation by a 980 nm laser: (a) pH = 1.5; (b) pH=2.0; (c) pH=2.5. The inset shows the photograph of the samples prepared at different pH values under 980 nm laser excitation (left) and the variation of the green and red upconversion luminescence at different pH values (right). The laser power for excitation was fixed at 250 mW.

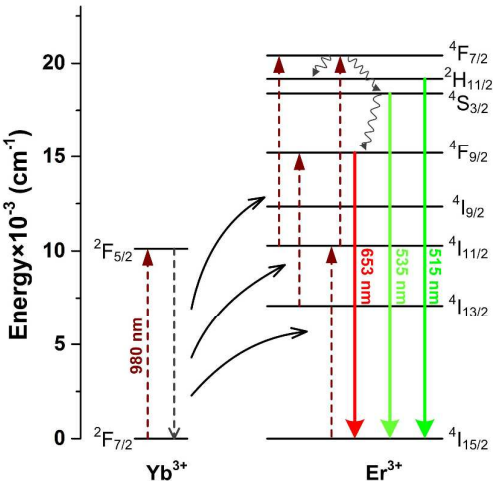

Fig. 8 Schematic illustration of energy-level diagram of Yb^{3+}, Er^{3+} and mechanism of upconversion emissions.